Supporting information

# Is Electron ping-pong limiting the catalytic hydrogen evolution activity in covalent photosensitizer-polyoxometalate dyads?

Yusen Luo,[a,b,†] Salam Maloul,[c,†] Maria Wächtler,[a,b] Andreas Winter,[d,e] Ulrich S. Schubert,[d,e] Carsten Streb*[c] and Benjamin Dietzek*[a,b,e]

[a]*Institute of Physical Chemistry and Abbe Center of Photonics, Friedrich Schiller University Jena, Helmholtzweg 4, 07743 Jena, Germany*

[b]*Department Functional Interface, Leibniz Institute of Photonic Technology (IPHT), Albert-Einstein-Strasse 9, 07745 Jena, Germany*

[c]*Institute of Inorganic Chemistry I, Ulm University, Albert-Einstein-Allee 11, 89081 Ulm, Germany*

[d]*Laboratory of Organic and Macromolecular Chemistry (IOMC), Friedrich Schiller University Jena, Humboldtstrasse 10, 07743 Jena, Germany*

[e]*Center for Energy and Environmental Chemistry Jena (CEEC Jena), Friedrich Schiller University Jena, Philosophenweg 7a, 07743 Jena, Germany*

[†]*Both authors contributed equally to the manuscript*

[*]*Corresponding authors: carsten.streb@uni-ulm.de*

*benjamin.dietzek@leibniz-ipht.de*

## Experimental details

The sample synthesis is reported elsewhere.[1,2] All spectroscopic and electrochemical experiments were performed at room temperature. The samples were dissolved in anhydrous DMF (Sigma-Aldrich) containing 0.1 M tetra-*n*-butylammonium tetrafluoroborate ($TBABF_4$) as electrolyte.

**Electrochemistry and Spectroelectrochemistry.** Cyclic voltammetry (CV) and spectro-electrochemistry (SEC) measurements were performed in a home-built three-electrode thin-layer cell with a path length of 1 mm. The three-electrode system consists of a glassy carbon working electrode, a platinum wire counter electrode and an Ag/AgCl pseudo-reference electrode. CV and potential-controlled monitoring were performed using a computer-controlled potentiostat (VersaSTAT 3, Princeton Applied Research). All potentials given in the manuscript refer to the ferrocene/ferrocenium couple as internal standard. The corresponding UV-Vis spectra were recorded on a single-beam spectrometer (Avantes, Avalight-DH-S-BAL).

**Time-resolved transient absorption spectroscopy.** Femtosecond (fs) transient absorption (TA) spectra were collected by using a previously reported home-built pump-probe laser system which is based on an amplified Ti: Sapphire oscillator (Libra, Coherent Inc.).[3] All compounds were excited by pump pulse centered at 395 nm produced by the second harmonic generation of the laser fundamental (790 nm, ~110 fs, 1 kHz) with a BBO crystal. The power of the pump beam was kept at 0.45 mW and the beam diameter of the pump was 760 µm at the sample position. This corresponds to $0.39 \times 10^{19}$ photons $m^{-2}$ per pulse. A white light supercontinuum generated by focusing a fraction of the fundamental in a rotating $CaF_2$ plate is used to probe the samples in a wide spectral range (340 to 700 nm). The probe beam is delayed in time with respect to the pump beam by means of an optical delay line and the polarization between probe and pump is set at the magic angle (54.7°). Transient absorption data were displayed after chirp correction. The transient absorption data were analyzed by a global multi-exponential fit (by using a customized software, Pascher Instruments AB, Sweden) after exclusion of a temporal window of 200 fs around time-zero in order to avoid contributions of the coherent-artifact region to the data analysis.[4] Furthermore, a spectral band of 20 nm around the pump-wavelength is omitted from the data analysis due to pump-scatter in this spectral range.

Detailed procedures of the TA measurements carried out under potentials can be found in the literature.[5,6] Briefly, the same home-built three-electrode cell with a path length of 1 mm was used. The pump and probe beam pass collinearly through a 1-mm hole in a 0.4 mm thick glassy carbon working electrode. The cell was purged with nitrogen for 5 to 10 min before adding the solution. Samples were pre-dissolved in anhydrous DMF ($OD_{395\,nm} = 0.45$) containing 0.1 M $TBABF_4$ as electrolyte. Solution was degassed with nitrogen for 10 to 20 min prior to transferring into the cell. Before each TA

measurement, a CV of the sample (scan rate: 0.05 V/s) was collected (*vs.* Ag/AgCl pseudo-reference electrode) to identify the proper reduction potential (the first reduction of the POM) to apply for the TA-SEC measurement. Then, a chronoamperometry (CA) measurement was started. After the current reached a plateau (ca. 3 min) TA measurement started. Only measurements recorded under a constant current were used for analysis.

Photocatalytic hydrogen evolution

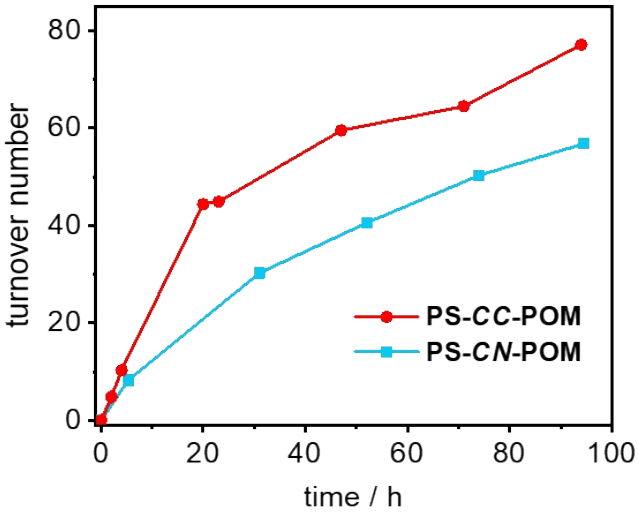


**Figure S1.** Hydrogen evolution activity of **PS-*CC*-POM** and **PS-*CN*-POM** under the same experimental conditions: PS-POM dyad (0.1 mM) were combined with a proton donor (acetic acid, 0.2 M) and electron donor (triethyl amine, 1 M) in water-free, deaerated N,N-dimethyl formamide (DMF). The reaction solution was irradiated using a light-emitting diode (LED) ($\lambda_{max}$ = 470 nm) at 25 °C and hydrogen evolution was quantified using calibrated head-space gas chromatography (GC). Each data point was recorded in duplicate. Considering less than 100 TON was produced in more than 100 h of LED irradiation, the overall quantum effeciency (QE) of both dyads is estimated to be significantly lower than 1%.

fs transient absorption spectra of **PS**

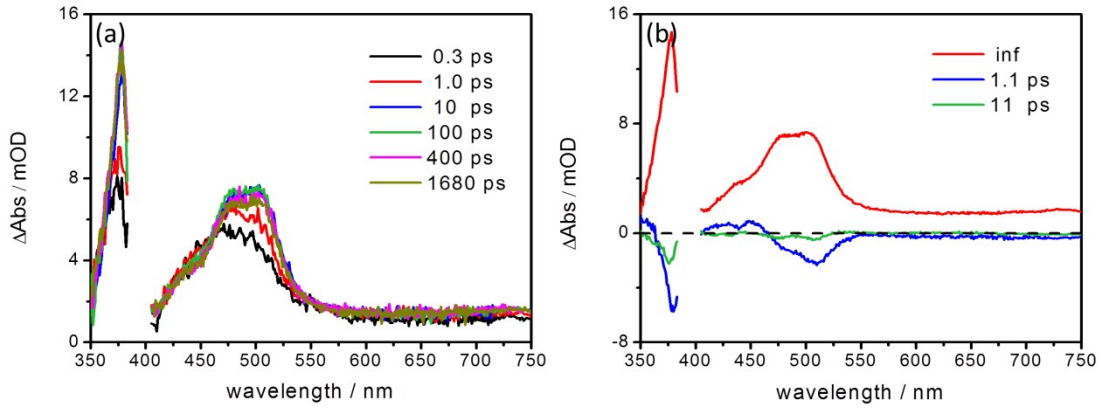


**Figure S2.** (a) fs TA spectra of **PS** at certain delay times collected upon excitation at 395 nm in DMF. (b) Decay-associated spectra (DAS) resulted from the global fit of the fs TA data.

The first component ($\tau_1$ = 1.1 ps) is assigned to the vibrational cooling of the hot $^3$MLCT states. The second component ($\tau_2$ = 11 ps) is attributed to the interligand electron transfer from an upper-lying $^3MLCT_{ppy}$ to the lower-lying $^3MLCT_{bpy}$ state. The infinite component represents the decay of the thermalized lowest $^3MLCT_{bpy}$ state. The assignment was discussed in detail in ref.7.

Comparison of the fs transient absorption results of **PS-*CN*-POM and PS-*CN*-POM$^{\bullet-}$**

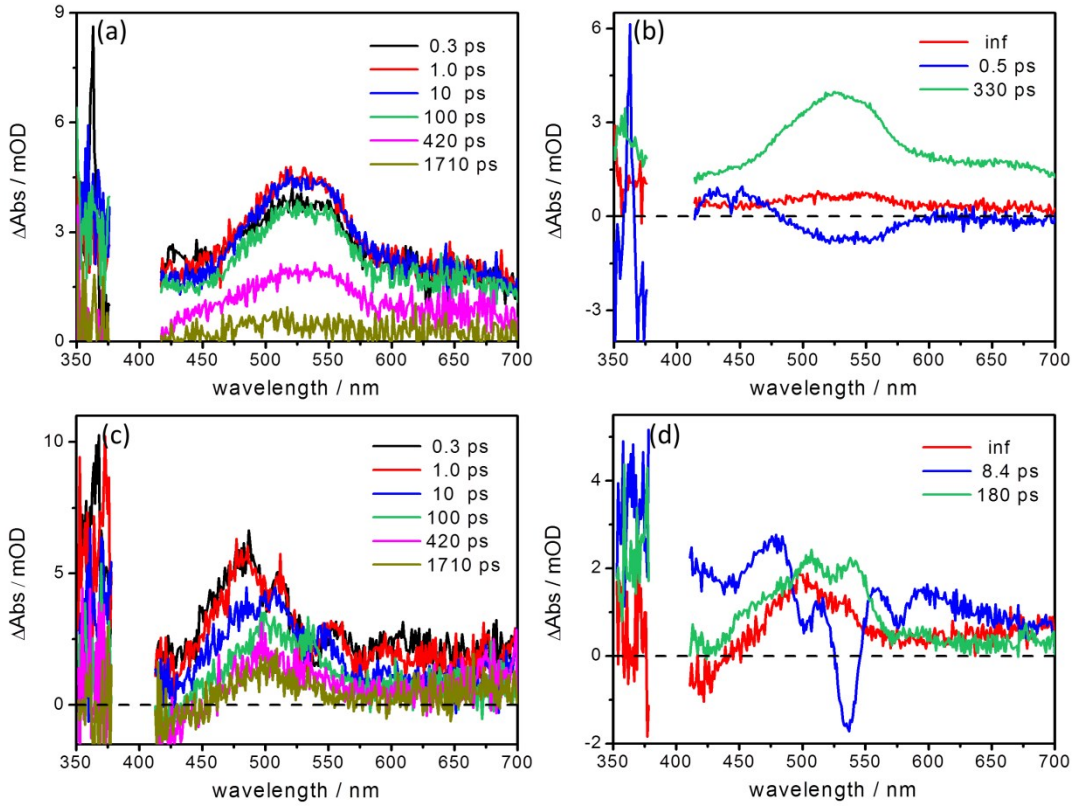


**Figure S3.** fs TA spectra of (a) **PS-*CN*-POM** and (c) **PS-*CN*-POM$^{\bullet-}$** (electrochemically pre-loaded with an electron on the POM unit) at certain delay times collected upon excitation at 395 nm in DMF with 0.1 M $TBABF_4$ electrolyte. (b) and (d) Decay-associated spectra (DAS) resulted from the global fit of the fs TA data.

The fs transient absorption spectra (c) and the decay-associated spectra (d) of the reduced species **PS-*CN*-POM$^{\bullet-}$** are quite different to the non-reduced one. This indicates the dominant contribution from the reduced species to the TA signal (Figure S3c) acquired under reductive potentials, pointing to a high electrochemical conversion.

Comparison of the fs transient absorption results of **PS-*CC*-POM and PS-*CC*-POM$^{\bullet-}$**

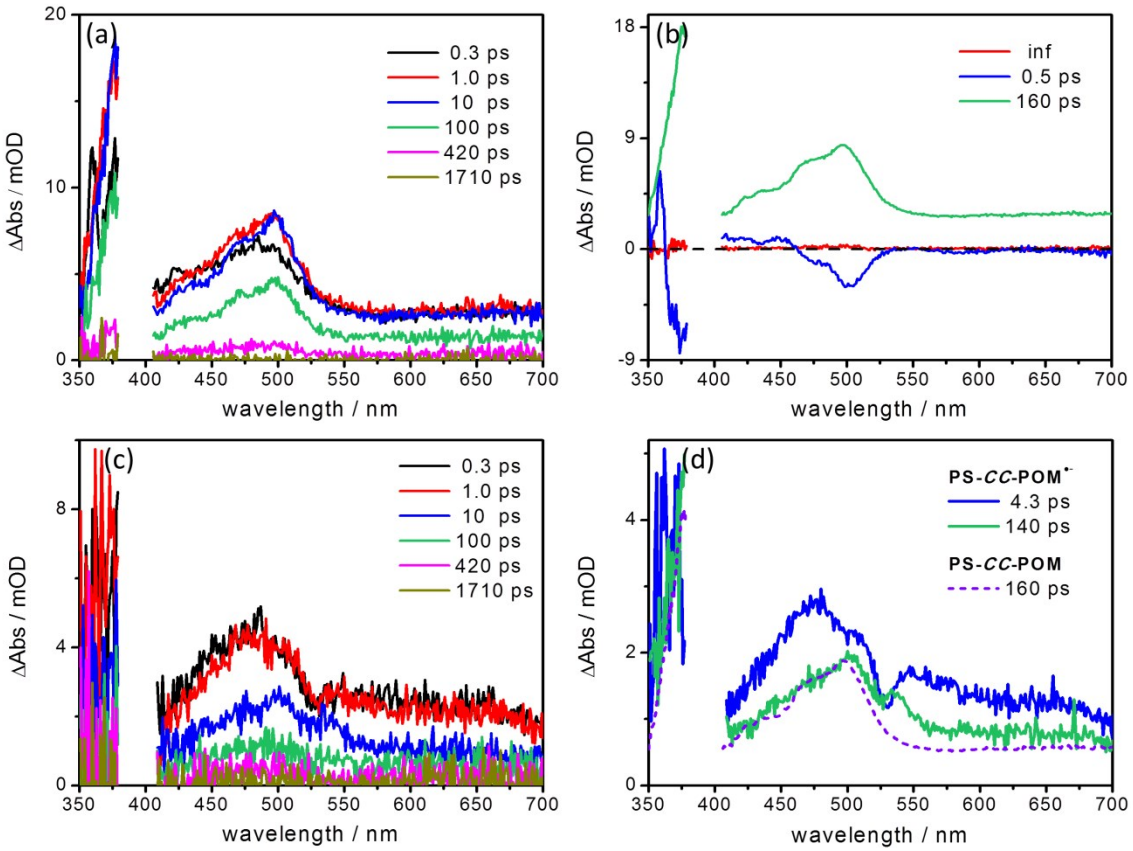


**Figure S4.** fs TA spectra of (a) **PS-*CC*-POM** and (c) **PS-*CC*-POM$^{\bullet-}$** (electrochemically pre-loaded with an electron on the POM unit) at certain delay times collected upon excitation at 395 nm in DMF with 0.1 M $TBABF_4$ electrolyte. (b) and (d) Decay-associated spectra (DAS) resulted from the global fit of the fs TA data.

Contributions from the electrochemically non-reduced species cannot be excluded for the TA results of **PS-*CC*-POM$^{\bullet-}$**. This is due to the fact that $\tau_2$ = 140 ps is quite close to $\tau_2$ = 160 ps observed for **PS-*CC*-POM** and both DAS ($\tau_2$) show nearly identical spectral shape below 500 nm (Figure S4d).

Relaxation scheme of the non-reduced species

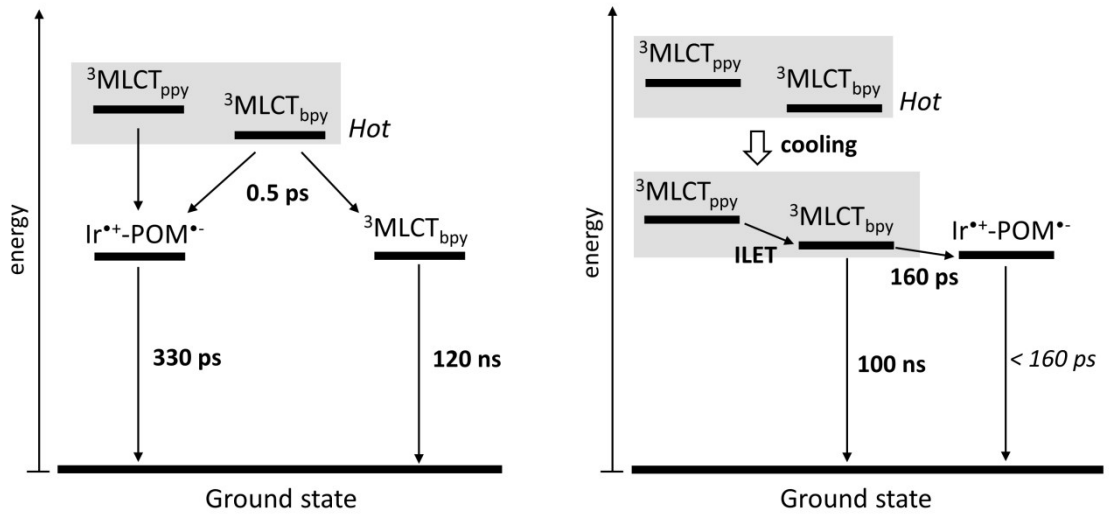


**Scheme S1.** Schematic representation of the proposed relaxation pathways for the non-reduced species **PS-*CN*-POM** (left) and **PS-*CC*-POM** (right) upon photoexcitation at 395 nm (*i.e.* excitation of the $^1$MLCT transitions). Due to the temporal resolution (~110 fs) of the fs TA setup and our data-processing (a temporal window of 200 fs around time-zero was excluded to avoid contributions of coherent artifacts) any ultrafast processes taking place within 200 fs cannot be probed. Hence, the photophysical models presented here only focus on the decay of the $^3$MLCT states.

For **PS-*CN*-POM** (left), ultrafast electron transfer occurs concertedly with vibrational cooling of the $^3$MLCT states ($\tau_1$ = 0.5 ps, Figure S3b).[7] The lifetime of the residual thermalized $^3$MLCT$_{bpy}$ state was obtained by the ns TA spectroscopy.[7] For **PS-*CC*-POM** (right), the fastest process ($\tau_1$ = 0.5 ps, Figure S4b) represents vibrational cooling within the hot $^3$MLCT states and interligand electron transfer (ILET) from the upper-lying $^3$MLCT$_{ppy}$ to the lower-lying $^3$MLCT$_{bpy}$ state.[7] Efficient (> 99%) charge separation takes place in **PS-*CC*-POM**, and hence, there is barely any long-lived signal left.

UV/Vis spectroelectrochemistry of **PS**

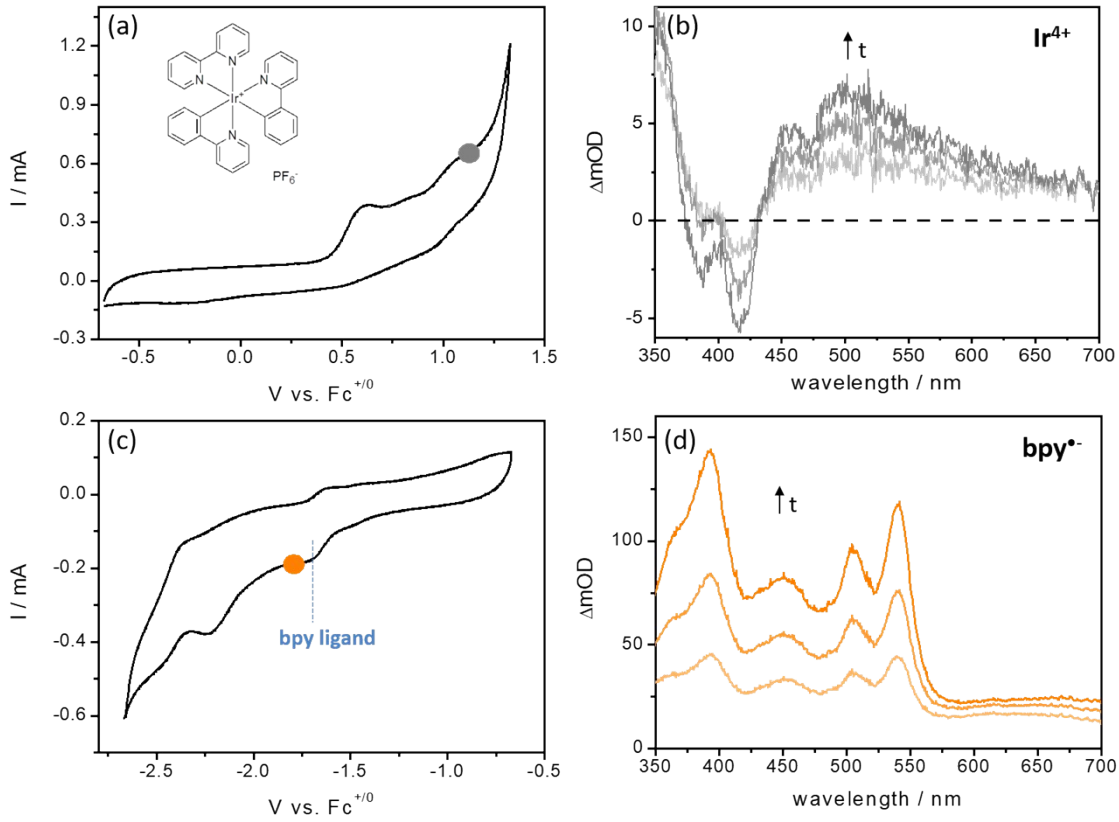


**Figure S5.** Cyclic voltammograms of (a) oxidation and (c) reduction of $[Ir(bpy)(ppy)_2]^+$ complex in DMF (0.1 M $TBABF_4$). Potential are given *vs.* $Fc^{+/0}$. The scan rate is 0.05 V/s. (b) and (d) Spectroelectrochemical UV/Vis absorption difference spectra of (a) oxidized Ir (*i.e.* $Ir^{4+}$) and (c) reduced bpy ligand (*i.e.* $bpy^{\bullet-}$). Potential applied to obtain the UV/Vis SEC are shown by dots on the CV curves.

UV/Vis spectroelectrochemistry of **PS-*CN*-POM**

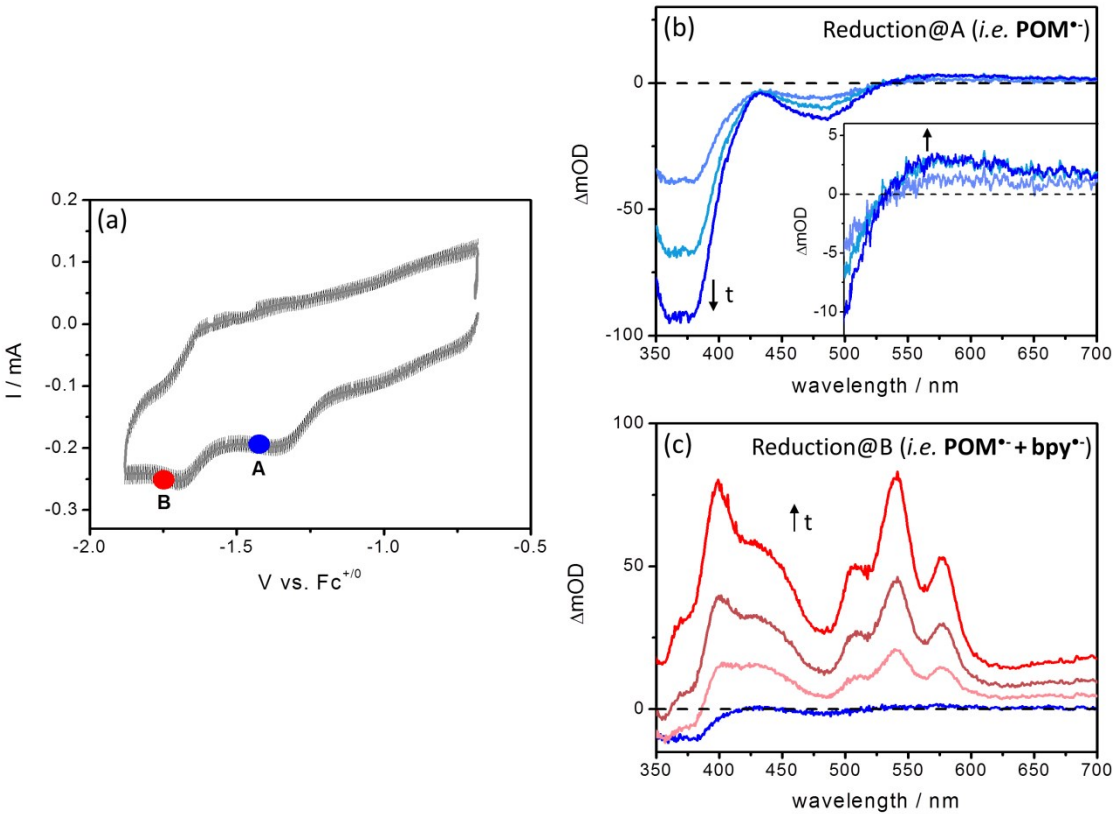


**Figure S6.** (a) Cyclic voltammogram of reduction of **PS-*CN*-POM** in DMF (0.1 M $TBABF_4$). Potential are given *vs.* $Fc^{+/0}$. The scan rate is 0.05 V/s. Spectroelectrochemical UV/Vis absorption difference spectra of (b) reduced POM (*i.e.* $POM^{\bullet-}$) and (c) reduced bpy ligand (*i.e.* $bpy^{\bullet-}$). Potential applied to obtain the UV/Vis SEC are shown by dots on the CV curves.

## Calculations of the energies of the intermediates

**Table S1.** Redox potentials (*vs.* $Fc^{+/0}$) of the individual components in PS-POM dyads in DMF (scan rate: 0.05 V/s).

| | **PS-*CN*-POM** | **PS-*CC*-POM**[b] |
|---|---|---|
| $PS^{+/0}$ | 0.90[a] | 0.83 |
| $PS^{0/-}$ | –1.67 | –1.85 |
| $POM^{0/-}$ | –1.35 | –1.23 |
| $POM^{-/2-}$ | –2.50[c] | –2.50[c] |

[a] taken from ref. 8, recorded with a scan rate of 0.1 V/s. [b] taken from ref. 1, recorded with a scan rate of 0.2 V/s. [c] taken from ref. 2, recorded with a scan rate of 0.1 V/s. Note: the second reduction of POM was acquired from the individual POM unit since the reduction of ppy ligand occurs at the same range (–2.4 ~ –2.6 V) which cannot be distinguished in the PS-POM dyads.

1) PS-*CN*-POM and PS-*CC*-POM, the energy is set to 0.00 eV.

2) The electrochemically reduced species, PS-*CN*-$POM^{\bullet-}$ and PS-*CC*-$POM^{\bullet-}$, the energies are 1.35 and 1.23 eV, respectively.

3) PS*-*CN*-$POM^{\bullet-}$ and PS*-*CC*-$POM^{\bullet-}$, the energies are 3.75 (*i.e.* 2.40 + 1.35 eV) and 3.63 eV (*i.e.* 2.40 + 1.23 eV), respectively. The energy of the excited PS (2.40 eV) corresponds to the lowest thermalized $^3$MLCT excited state of $[Ir(bpy)(ppy)_2]^+$.[9]

4) $PS^{\bullet+}$-*CN*-$POM^{2\bullet-}$ and $PS^{\bullet+}$-*CC*-$POM^{2\bullet-}$, the energies are 4.75 (*i.e.* 0.90 + 1.35 + 2.50 eV) and 4.56 eV (*i.e.* 0.83 + 1.23 + 2.50 eV), respectively.

5) $PS^{\bullet-}$-*CN*-POM and $PS^{\bullet-}$-*CC*-POM, the energies are 1.67 and 1.85 eV, respectively.

Reorganization energy

$$\lambda = \lambda_i + \lambda_o \quad (1)$$

$$\lambda_o = \frac{e^2}{4 \cdot \pi \cdot \varepsilon_0} \cdot \left(\frac{1}{2a_1} + \frac{1}{2a_2} - \frac{1}{R_{DA}}\right) \cdot \left(\frac{1}{n^2} - \frac{1}{\varepsilon_s}\right) \quad (2)$$

where $\lambda_i$ and $\lambda_o$ represent the inner and outer reorganization energy, respectively.[10,11] $\lambda_i$ reflects the free energy change associated with the nuclear bond length changes within molecules and $\lambda_o$ accounts for the reorganization of the surrounding chemical environment, *e.g.* solvent molecules. In the simplest model, electron donor and acceptor are treated as spheres with radii $a_1$ and $a_2$.[10,11] $R_{DA}$ is the donor-acceptor distance. n (1.4305) and $\varepsilon_s$ (36.71) represent refractive index and dielectric constant of the solvent DMF, respectively. $\varepsilon_0$ is the vacuum permittivity ($8.85 \times 10^{-12}$ F/m).

For the PS-POM dyads:

1. $\lambda_i$ is treated to be 0.1 eV[10,11] and is commonly considered as distance[10] independent.

2. The radii of PS and POM were obtained from their single crystal structures. For the Ir(III) photosensitizer, the radius is between 4.8 and 5.8 Å:

| | |
|---|---|
| Distance between Ir and C(ppy) | 4.8077 Å |
| Distance between Ir and H(ppy) | 5.7549 Å |
| Distance between Ir and C(bpy) | 4.8962 Å |
| Distance between Ir and H(bpy) | 5.8452 Å |

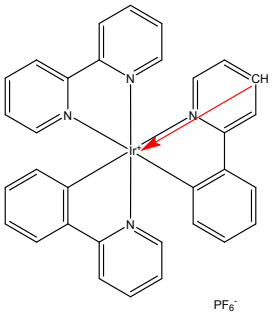


3. The center-to-center distance $R_{DA}$ for the species **PS-*CC*-POM** and **PS-*CN*-POM** are 9.3 and 11.4 Å, respectively.

## Reference


1. A. Winter, P. Endres, E. Schröter, M. Jäger, H. Görls, C. Neumann, A. Turchanin and U. S. Schubert, *Molecules*, 2019, **24**, 4446.

2. S. Schönweiz, M. Heiland, M. Anjass, T. Jacob, S. Rau and C. Streb, *Chem. Eur. J.*, 2017, **23**, 15370–15376.

3. J. Kübel, R. Schroot, M. Wächtler, U. S. Schubert, B. Dietzek and M. Jäger, *J. Phys. Chem. C*, 2015, **119**, 4742–4751.

4. B. Dietzek, T. Pascher, V. Sundström and A. Yartsev, *Laser Phys. Lett.*, 2007, **4**, 38–43.

5. S. Bold, L. Zedler, Y. Zhang, J. Massin, V. Artero, M. Chavarot-Kerlidou and B. Dietzek, *Chem. Commun.*, 2018, **54**, 10594−10597.

6. L. Zedler, A. K. Mengele, K. M. Ziems, Y. Zhang, M. Wächtler, S. Gräfe, T. Pascher, S. Rau, S. Kupfer and B. Dietzek, *Angew. Chem. Int. Ed.*, 2019, **58**, 13140–13148.

7. Y. Luo, S. Maloul, S. Schönweiz, M. Wächtler, C. Streb and B. Dietzek, *Chem. Eur. J.*, 2020, **26**, 8045–8052.

8. S. Schönweiz, S. A. Rommel, J. Kübel, M. Micheel, B. Dietzek, S. Rau and C. Streb, *Chem. Eur. J.*, 2016, **22**, 12002–12005.

9. S. Ladouceur, D. Fortin and E. Zysman-Colman, *Inorg. Chem.*, 2010, **49**, 5625–5641.

10. M. Kuss-Petermann and O. S. Wenger, *Phys. Chem. Chem. Phys.*, 2016, **18**, 18657−18664.

11. E. Göransson, J. Boixel, J. Fortage, D. Jacquemin, H.-C. Becker, E. Blart, L. Hammarström and F. Odobel, *Inorg. Chem.*, 2012, **51**, 11500−11512.